APPLIED PHYSICS REVIEWS—FOCUSED REVIEW

Vertically aligned carbon based varactors

Farzan A. Ghavanini,[a] Peter Enoksson, Stefan Bengtsson, and Per Lundgren
Microtechnology and Nanoscience Department (MC2), Chalmers University of Technology, Göteborg, Sweden

This paper gives an assessment of vertically aligned carbon based varactors and validates their potential for future applications. The varactors discussed here are nanoelectromechanical devices which are based on either vertically aligned carbon nanofibers or vertically aligned carbon nanotube arrays. A generic analytical model for parallel plate nanoelectromechanical varactors based on previous works is developed and is used to formulate a universal expression for their voltage-capacitance relation. Specific expressions for the nanofiber based and the nanotube based varactors are then derived separately from the generic model. This paper also provides a detailed review on the fabrication of carbon based varactors and pays special attention to the challenges in realizing such devices. Finally, the performance of the carbon based varactor is assessed in accordance with four criteria: the static capacitance, the tuning ratio, the quality factor, and the operating voltage. Although the reported performance is still far inferior to other varactor technologies, our prognosis which stems from the analytical model shows a promise of a high quality factor as well as a potential for high power handling for carbon based varactors. © *2011 American Institute of Physics*. [doi:10.1063/1.3583536]

TABLE OF CONTENTS

I. INTRODUCTION

The synthesis of one-dimensional carbon nanostructures have been under constant development since their discovery. This development has resulted in a variety of different techniques such as laser ablation,[1,2] arc discharge,[3,4] thermal chemical-vapor deposition (TCVD),[5–7] and plasma-enhanced chemical-vapor deposition (PECVD).[8–10] The laser ablation and the arc discharge techniques are efficient methods for producing large quantities of high-quality carbon nanotubes (CNTs) but they do not provide any control over the spatial arrangement of the resulting material[11] and therefore exhaustive post-growth processing is required to disentangle, redeposit, and align the nanotubes in order to fabricate a device.[12,13] On the other hand, catalytic TCVD and PECVD techniques allow for a more deterministic synthesis process.[11] In the case of the TCVD process, it is possible to grow a dense forest of CNTs known as vertically aligned carbon nanotube array (VANTA). Although individual CNTs cannot be aligned vertically, they can support each other to collectively grow perpendicular to the substrate; a phenomenon known as the crowding effect.[14] It should be noted that, while it is not possible to precisely control the shape of individual CNTs in a VANTA, the size, the height, and the alignment of the VANTA itself can be controlled accurately. In contrast to the TCVD process, the PECVD process offers determinism at the level of individual nanostructures, which are often referred to as vertically aligned carbon nanofibers (VACNFs). Nanofibers are distinguished from nanotubes by their internal structure which consists of stacked nano-cones or nano-cups made up of graphene. The stacked nano-cone structure is often referred to as "herringbone," while the stacked nano-cup structure is known as the "bamboo" type.[11]

Since carbon nanostructures have started to stand on their feet in the form of VACNFs and VANTAs, they have provided an unprecedented opportunity to realize a new bottom-up-engineered material with excellent mechanical and electrical properties which could exploit the third dimension

a)Electronic mail: farzan@chalmers.se.

at a reasonable cost. It came as no surprise to see the new material being employed in a large spectrum of applications, from thermal interfaces[15] and flip-chip bumps[16] to electron emitters[17–19] and gene delivery arrays.[20,21] The achievements during the last few years in reproducible synthesis of high quality VACNFs and VANTAs have extended the boundaries of their application to the realm of nanoelectromechanical systems (NEMS). Although carbon nanotubes and nanofibers had already been used in horizontal configuration as nanoelectromechanical devices,[22–30] this time their as-grown vertical alignment was exploited. Good examples of such devices include nanoelectromechanical switches[31] and the nanoscale memory cell[32] based on VACNFs.

In this report, we focus on a novel application of VACNFs and VANTAs: a NEMS varactor. A varactor is a two-terminal device the capacitance of which depends on the voltage applied to its terminals. Varactors are mainly used in radio frequency systems such as voltage controlled oscillators (VCOs),[33] and frequency multipliers.[34] The varactor technology is dominated by solid-state devices realized in silicon or GaAs. The advancement in micromachining technologies in the last twenty years has introduced the new class of microelectromechanical (MEMS) varactors.[35,36] However, the development of MEMS varactors has not progressed at the pace of other MEMS devices, which can be explained by the abundance of discrete high quality factor silicon and GaAs varactors up to 30 GHz.[37] But there is still a pressing need for electromechanical varactors including the novel NEMS varactors: they have the potential of very high quality factors, they can be designed to withstand large radio frequency (rf) voltage swings, they exhibit a symmetric capacitance-voltage (C-V) response, and they can be inexpensively produced on top of high-resistivity silicon substrates.[37]

The aim of this work is to give a general assessment of carbon based NEMS varactors and to validate their potential using an analytical model developed here, as well as published experimental data.[38–43] Since carbon based varactors are still in emergence, this review focuses on their potential advantages and remaining challenges. First, a short review of existing varactor technologies is given. Then a detailed description of carbon based varactor fabrication is presented. At the end, we evaluate their performance using the key parameters: tuning ratio, quality factor, static capacitance, and operating voltage.

II. PRINCIPLE OF OPERATION

A. Continuous tunable capacitors

The capacitance of a parallel plate capacitor which consists of two conductors separated by a nonconductive region is given by the following equation (neglecting the fringing field):[44]

$$C = \varepsilon_0 \varepsilon_r \frac{A}{d} \quad (1)$$

where ε_0 is the permittivity of free space, ε_r is the relative permittivity of the nonconductive region, A is the overlapping area of the conductors, and d is the gap between them.

Except for the permittivity of space which is a universal constant, $\varepsilon_0 = 8.85 \times 10^{-12}$ F/m, any of the three other parameters can be used to tune the capacitance value.

The most widely used type of tunable capacitors are the varactor diodes[45] in which the depletion region acts as the gap between the conducting electrodes. In the case of Schottky diodes, the depletion layer is created at the semiconductor side of a metal-semiconductor junction[46] while in a *p-n* junction diode the depletion layer is distributed over the junction as a function of the doping profile.[47] To tune the resulting capacitance, the width of the depletion region is modified by applying a proper reverse bias. The heterostructure barrier varactor (HBV) is another type of varactor taking advantage of the bias dependency of the depletion region which, in this case, is created between two different semiconducting materials.[48]

Another way of making a varactor is to sandwich a ferroelectric material between a pair of electrodes. Since the relative permittivity of ferroelectric materials strongly depends on the applied electric field, a bias voltage can alter the capacitance of the resulting device.[49] This device is referred to as a ferroelectric varactor.

A radically different approach, utilized in microelectromechanical systems, is to change the geometrical configuration of a capacitor by mechanically moving the electrodes or the dielectric between them. In a parallel plate MEMS varactor, one[50,51] or two[35] suspended electrodes are moved toward a static electrode resulting in a reduced gap, thus increasing the capacitance. Alternatively, a dielectric slab suspended between two conductive electrodes can be displaced to alter the relative dielectric constant between the capacitor plates.[52] In an interdigital MEMS varactor, the overlapping length of the fingerlike structures is varied which alters the overlapped area of the capacitor.[53,54]

B. Switched capacitors

A switched capacitor is basically an on-off switch in series with a capacitor with a discrete C-V characteristic. Semiconductor devices with high performance at radio frequencies such as PiN diodes, CMOS switches, and pHEMT switches are typically used with low loss nontunable capacitors to fulfill high performance demands of those applications where continuous capacitance change is not required.[45] MEMS switched capacitors suitable for rf applications have also been developed.[37]

C. The carbon based varactor

Although the notion of a carbon based varactor was first published in 2007,[39] its prerequisites had already been available for a couple of years. In 1999, Kim *et al.* used carbon nanotubes to create a pair of robust nano-tweezers that could be utilized for nanoscale manipulation and measurement.[55] Their device was made of a pair of CNTs which were grown *ex situ* and then transferred and attached on the tip of a tapered glass micropipette. The principle of operation was based on electrostatic attraction created by a bias voltage applied to the CNTs. Similar works were reported by other groups who employed *ex situ* grown carbon nanofibers[56] and

carbon nanotubes[57,58] to realize standing nano-tweezers or switches. In 2008, when the PECVD synthesis of carbon nanostructures had matured, Jang *et al.* presented the first NEMS switch using *in situ* grown VACNFs.[31] This work was a major breakthrough since it clearly demonstrated the potential of VACNFs for a new generation of nano-scale devices. Another implication of this work was the fact that the deterministic nature of the PECVD process could be exploited to grow a large number of VACNFs at predefined positions to compose a two terminal device with measurable capacitance; the carbon based varactor was prepared for conception.

As explained in the Introduction, the synthesis determinism is achieved in form of VACNFs and VANTAs and therefore, both structures can be used to realize varactors. Figure 1 shows the generic form of a VACNF-based and a VANTA-based varactor. Using their resemblance to daily objects, one could name the former "comblike" and the latter "brushlike" varactor. Both of these varactors share the same principle of operation; a bias voltage applied on their terminals creates an electrostatic field which exerts a bending moment on the charged VACNFs or VANTAs. Consequently, the gap between the two parallel walls is reduced and the capacitance is increased. Since the reduction in the gap depends on the strength of the electrostatic field and therefore the applied bias voltage, a voltage-dependent capacitance is obtained.
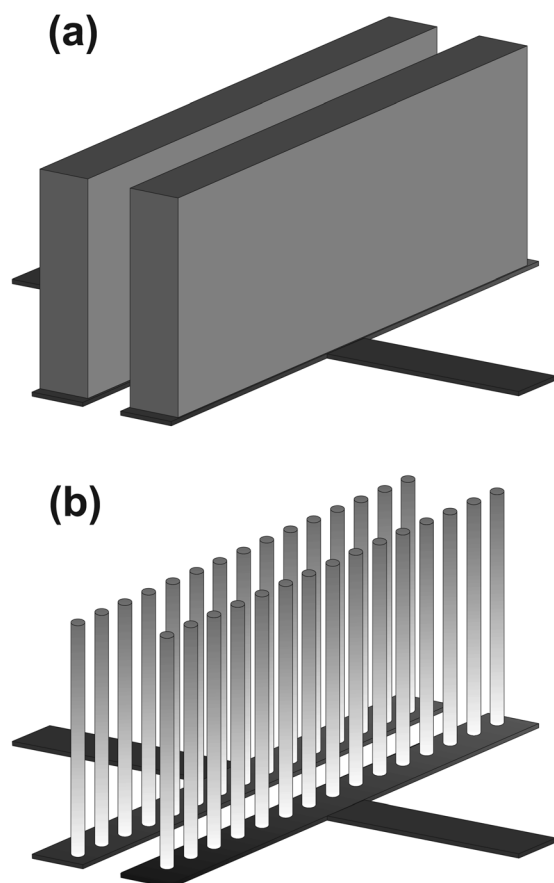

FIG. 1. The schematic presentation of (a) the brushlike (VANTA-based) and (b) the comblike (VACNF-based) varactor.

III. MODELING

Physics and mechanics of one-dimensional carbon nanostructures are not new fields. Many years of research have led to improved understanding of the nanoelectromechanical systems based on CNTs and CNFs in terms of the interactions involved as well as the validity of the application of macroscopic models.[31,32,58–61] In this paper, we apply this knowledge to identify the active forces in the carbon based varactor and to model their influence. First, we develop such a model for a generic one-dimensional system. Then, the generic model is expanded separately for the brushlike and the comblike varactors.

VACNFs and VANTAs grown in a CVD process are weakly attached to the substrate rendering the substrate interface the weakest point in the whole structure.[62] This explains why they typically break at their bases by horizontal shear along graphite planes when lateral force is exerted on them.[63] Nevertheless, in applications such as the varactor where the lateral force is not directly applied to the interface one could assume that they behave as vertical cantilever beams clamped at their base.[31,32] Continuum beam theory has been used widely to model singly- and doubly-clamped carbon nanostructures.[31,32,58,59,61,64–68] Dequesnes *et al.* have used molecular dynamics (MD) to establish the accuracy of continuum beam theory.[59] Their results showed a very good agreement with the beam theory when the length to diameter ratio of the nanotubes was larger than ten, which indeed is the case for practical applications.

Another important factor in modeling the varactor is the electrical properties of the incorporated material. Zhang *et al.*[69] as well as other groups[70–72] have investigated the current-voltage (I-V) characteristic of individual VACNFs using accurate four-point probe measurements and showed that they exhibit linear behavior. They observed an average VACNF resistivity of 4.23×10^{-3} Ω·cm which is consistent with a simple model of charge transport where electrons travel mainly from one graphitic plane to another along the length of the nanofiber. Therefore, VACNFs can be approximated as cylindrical conductors.[59] This is not as straightforward in the case of VANTAs; a VANTA composed of SWNT is less electrically conductive than one made of MWNT.[73] This trend stems from the fact that a SWNT forest includes a large population of semiconducting single-wall carbon nanotubes while MWNT forests are mainly composed of metallic few-walled carbon nanotubes. Hence, MWNT based VANTAs are the preferred choice for applications with a demand for high electrical conductivity (as for the case of a varactor). When modeling the constituents as conductors, the electronic charges distribute themselves on the surface of a VACNF or a VANTA so as to produce an equipotential surface. Therefore, the electrostatic forces can be computed by using conventional capacitance expressions.[44]

Before continuing to the next section one comment is in place regarding the van der Waals interaction between two oppositely charged VACNFs or VANTAs. Dequesnes *et al.* have used the continuum model to compute the deflection of cantilever beams with and without van der Waals forces.[59] For instance, they have shown that for a singly clamped
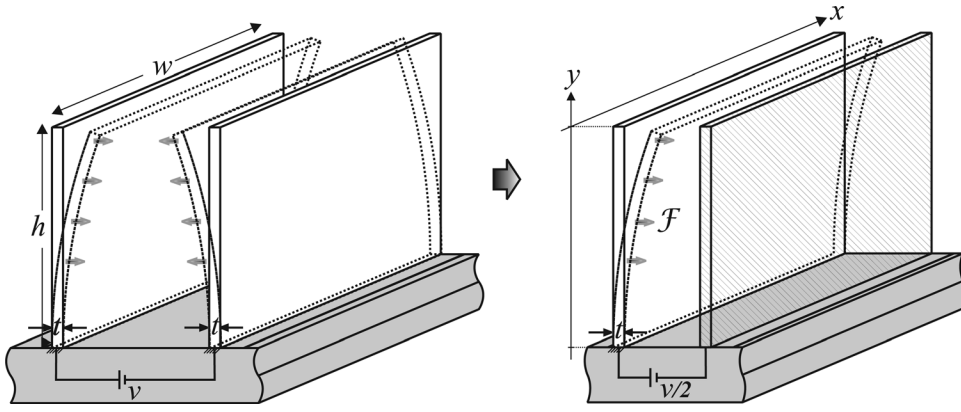
FIG. 2. The generic two-dimensional NEMS varactor model. The electrostatic force is represented by an arbitrary function **F**.

SWNT with a length of 50 nm and a diameter of 2 nm, the effect of van der Waals forces disappears when the initial gap is more than a few nanometers. Although the degree of influence of van der Waals forces depends on the geometrical configuration of the nanostructures and the strength of other forces involved, they can generally be ignored in practical applications where the initial gap is more than 30 nm.[66] In the following modeling, we do not consider the van der Waals forces between the VACNFs and VANTAs since we assume that the initial gap is large enough to render the electrostatic interaction dominant. Within a single VANTA structure however, the van der Waals interaction between the individual CNTs contributes to achieving its vertical alignment.[74]

A. Generic NEMS varactor model

Figure 2(a) shows the generic NEMS varactor model composed of two conductive plates, clamped at their bases with height h, width w, and thickness t. The assumption that the plates are identical creates a symmetry permitting us to reduce the system to a single plate placed in front of an imaginary ground plane as shown in Fig. 2(b). The application of a bias voltage will exert an electrostatic force which can be represented by an arbitrary function **F** per unit area of the plate. The deflection at point (x, y) is denoted $u(x, y)$. Assuming that the thickness of the plate is much smaller than its lateral dimensions, the shape of the bent plate can be estimated using a classical plate equation:

$$\nabla^2 D \nabla^2 u(x, y) = F(u, x, y) \qquad (2)$$

where D is the flexural rigidity of the plate. The electrostatic force **F** in Eq. (2) is a nonlinear function of both position and deflection, making it difficult, in general, to come up with a closed-form solution.[59] However, a closed-form solution can be found if appropriate approximations are made.

In order to derive an analytical approximation the system in Fig. 2(b) is simplified to a one-dimensional lumped model as shown in Fig. 3. In the lumped model the curvature of the bent plate is ignored and the tip deflection is replaced by a uniform change in the gap between a rigid plate and an imaginary ground plane. In this setup, the restoring elastic force, F_{elas}, is expressed using an effective spring constant, k:

$$F_{elas} = -ku \qquad (3)$$

The effective spring constant is system dependent and should be calculated separately for the brushlike and the comblike varactor.

The electrostatic force, F_{elec}, for the parallel plate configuration of Fig. 3 is given by (note that the voltage between the plate and the ground plane is half the plate-to-plate voltage):

$$F_{elec} = \frac{\varepsilon_0 wh \left(\frac{V}{2}\right)^2}{2\left(\frac{g}{2} - u\right)^2} \qquad (4)$$

in which ε_0 is the permittivity of free space, V is the bias voltage applied between the plates, g is the original gap, and u is the uniform deflection. Finally, the deflection u for the applied voltage V is found from the equilibrium condition:

$$F_{elas} + F_{elec} = 0 \qquad (5)$$

Replacing F_{elas} and F_{elec} with their expressions and using,

$$C \equiv \frac{\varepsilon_0 wh}{(g - 2u)}; \quad C_0 \equiv \frac{\varepsilon_0 wh}{g} \qquad (6)$$

gives,

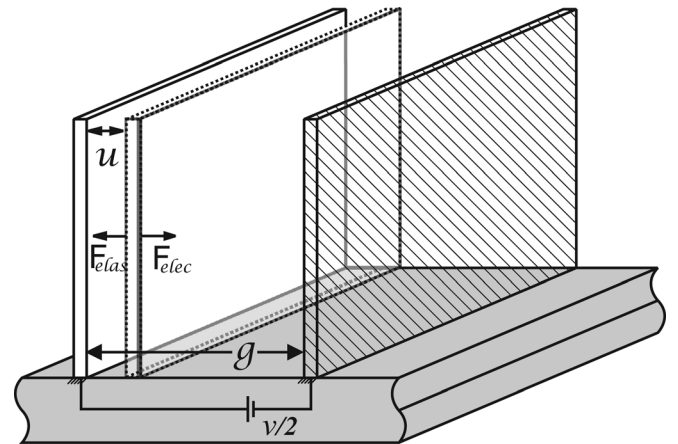$$\frac{C^2 V^2}{C_0 g} - k \cdot g \left(1 - \frac{C_0}{C}\right) = 0 \qquad (7)$$

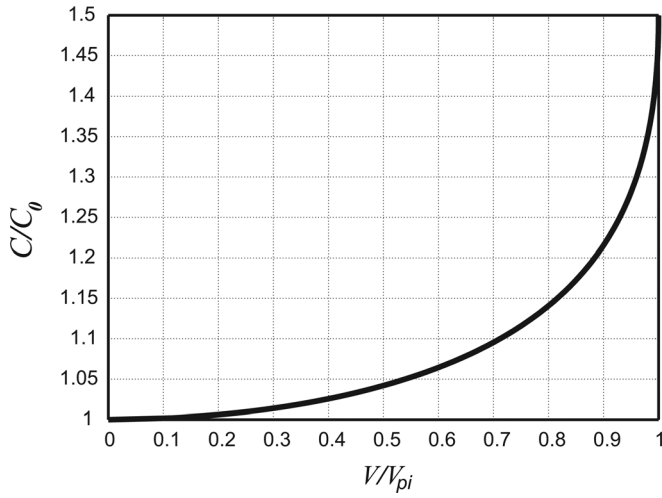FIG. 3. The one-dimensional lumped model of the NEMS varactor.

FIG. 4. The characteristic voltage-capacitance curve of NEMS varactor. The system becomes mechanically instable at the pull-in voltage and the electrodes snap into each other. This limits the maximum capacitance tunability in a standard NEMS varactor to 50%.

Ideally, one would try to solve Eq. (7) to find $C(V)$. Although it is possible to find such a solution, the outcome is not more intuitive than the readily available $V(C)$:

$$V = g\left(\frac{C_0}{C}\right)\sqrt{\frac{k}{C_0}\left(1 - \frac{C_0}{C}\right)} \qquad (8)$$

One important phenomenon that can already be observed from Eq. (8) is the mechanical instability that occurs at a certain applied voltage referred to as the pull-in voltage, V_{pi}. The pull-in voltage can be found from the condition $\partial V/\partial C = 0$ which gives,

$$V_{pi} = \sqrt{\frac{4}{27}\frac{k \cdot g^2}{C_0}} \qquad (9)$$

Combining Eq. (8) and (9) gives a universal, dimensionless expression for NEMS varactors,

$$\frac{V}{V_{pi}} = \left(\frac{C_0}{C}\right)\sqrt{\frac{27}{4}\left(1 - \frac{C_0}{C}\right)} \qquad (10)$$

Figure 4 illustrates the universal voltage-capacitance curve of a NEMS varactor. It clearly shows that the capacitance cannot be tuned to more than 50% of the initial value regardless of the design parameters; an inherent limitation imposed by the mechanical instability at the pull-in voltage.

B. Comblike varactor

Figure 5(a) shows the equipotential lines for a single pair of oppositely charged VACNFs at a cross-section level. In the case of two opposing rows of sparsely populated VACNFs, as depicted in Fig. 5(b), the electrostatic interaction between adjacent nanofibers alters the equipotential lines. As the distance between the adjacent VACNFs shrinks and eventually becomes much smaller than the gap between the opposing rows, the resulting electric potential field approaches that of a parallel plate capacitor. This can be seen in Fig. 5(c). As a result, one can replace a sufficiently
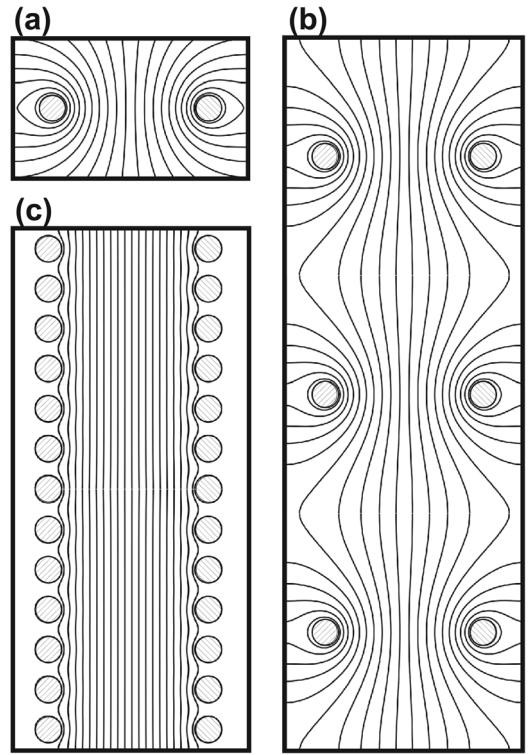

FIG. 5. The equipotential lines at a cross-section level between (a) a single pair of oppositely charged VACNFs, (b) two sparsely populated rows of VACNFs, and (c) two rows of densely populated VACNFs as simulated by COMSOL Multiphysics.

dense row of individual VACNFs with an equivalent conductive plate with a negligible error for field calculations. In a setup where the rows are separated by g and each row is composed of N nanofibers with diameter D, spacing S, and height h the capacitance is given by:

$$C_0 = \frac{\varepsilon_0 N(S + D)h}{g} \qquad (11)$$

The spring constant of a single VACNF under a uniform load is $k_f = 8EI/h^3$ where E, I, and h are the Young's modulus, the area moment of inertia, and the height of the nanofiber respectively. The effective spring constant of the equivalent plate, k_p, can be found by considering the spring constants of all the VACNFs in one row, in parallel:

$$k_p = Nk_f = \frac{8NEI}{h^3} \qquad (12)$$

By replacing the area moment of inertia, I, with $\pi D^4/64$ for a VACNF with diameter D, we arrive at:

$$k_p = \frac{\pi NED^4}{8h^3} \qquad (13)$$

Finally, replacing Eqs. (11) and (13) into Eq. (9), gives the pull-in voltage of a comblike varactor with sufficiently dense rows of individual VACNFs,

$$V_{pi} = \frac{D^2}{h^2}\sqrt{\frac{4\pi}{27\varepsilon_0}\frac{Eg^3}{(S + D)}} \qquad (14)$$

Another important issue that has to be considered in designing a comblike varactor is the mechanical resonances that occur at certain frequencies determined by the device configuration and mechanical properties of the nanofibers. Isacsson *et al.* have studied a system where a row of VACNFs is placed in front of an infinite conducting plane.[75] They showed that the mechanical resonances take place both in transverse modes where nanofibers oscillate toward the conducting plane and in longitudinal modes where nanofibers oscillate in the direction along the array. Although these oscillations can be exploited to design a frequency modulator or a tunable filter, they must be avoided when a plain capacitance tuning is expected from the varactor. The analytical model reported by Isacsson *et al.* provides the necessary basis for calculating these frequencies. The simple model given above can explain the varactor behavior as long as the driving frequency does not coincide with any of the resonance points.

C. Brushlike varactor

A brushlike varactor, as shown in Fig. 1(a), is composed of two parallel VANTAs. Despite the large number of studies regarding the mechanical properties of individual CNTs[76] very little is known about that of a VANTA structure. A recent study has shown that the nanotubes in a VANTA collectively form zigzag buckles that can fully unfold to their original length upon load release.[77] This indicates that a VANTA can be considered as a single mechanical structure with an effective elastic modulus. Therefore, assuming the lumped model, the spring constant of a VANTA with a rectangular cross-section under a uniform load can be given by:[78]

$$k_p = \frac{2}{3} \frac{Ewt^3}{h^3} \qquad (15)$$

where E is the effective Young's modulus of the VANTA, and w, t, and h are the VANTA's width, thickness, and height, respectively [see Fig. 2(a)]. Finally the pull-in voltage of a brushlike varactor is expressed by substituting Eq. (15) into the universal pull-in equation given in Eq. (9):

$$V_{pi} = \frac{1}{h^2} \sqrt{\frac{8}{81\varepsilon_0} Eg^3 t^3} \qquad (16)$$

IV. REALIZATION

A. Comblike varactor

VACNFs are most commonly grown in a direct-current glow discharge plasma enhanced CVD (dc PECVD) process. The vertical alignment of the fibers is a result of the electric field in the plasma.[11] Although other plasma sources such as hot-filament dc (HF-dc PECVD),[79] magnetron-type radio frequency (rf-PECVD),[80,81] inductively coupled plasma (ICP PECVD),[82] and microwave (M-PECVD)[83] have also been used to grow carbon nanotubes and aligned nanofibers, dc PECVD has produced the best results.[11] The VACNF growth recipe depends on the properties of the reactor being used and the choice of catalyst and underlayer materials. Melechko *et al.*[11,84] and Meyyappan *et al.*[85] give compre-

hensive reviews on the synthesis of VACNFs by PECVD process.

One of the main limitations of the dc PECVD growth reactors is the requirement that the substrate be electrically conductive. This limitation stems from the unidirectional nature of the plasma which leads to charge accumulation on nonconductive substrates. The charge accumulations result in plasma instabilities that prohibit the growth. This does not pose a problem as long as the growth is carried out on top of a metal film. However, when device fabrication is the goal, this metal film must be patterned. Hence, a large nonconductive surface of the substrate is exposed. One way around this problem is to do the metal patterning after the growth.[86] Although it may be an attractive solution for many cases, it is very challenging if post-growth nano-scale lithography is required as the VACNFs may interfere with the exposure process. Moreover, rf devices such as varactors must be fabricated using thick metal layers to minimize the losses.[37] The latter exposes the VACNFs to a long etching time needed to pattern the thick metal layer which would induce nonreversible damages to the carbon nanostructures. Ghavanini *et al.*, proposed another solution in which a very thin layer of Cr is first deposited on the substrate and then the thick metal pattern is transferred on top of the Cr layer in a lift-off process.[87] In this way, the thin Cr layer is removed after the growth in a short dry etching process with minimum damage to the VACNFs.

The tuning action of a comblike varactor is the result of uniform bending of a large number of VACNFs. This uniform deformation is not achieved unless the VACNFs themselves are uniform in terms of diameter and height. It has been shown that the diameter of a VACNF is directly correlated to the original size of the catalyst seed.[88,89] Moreover, the height of a VACNF has been shown to be a function of, among other things, the growth time as well as the catalyst size.[87] Therefore, in order to achieve the required uniformity, the catalyst material should be patterned to form seeds of roughly the same size as the desired VACNF diameter and therefore making the use of methods such as electron beam (e-beam) lithography inevitable.

The authors are currently pursuing the realization of the comblike varactor. Our process, as summarized in Fig. 6, includes two e-beam lithography steps, one for patterning the electrodes and one for patterning the catalyst seeds. We have adopted Ni as the catalyst material not only because it is known as an efficient catalyst for VACNF synthesis but also due to its compatibility with standard CMOS processes[90] – a crucial requirement for future integration with electronic circuitry. We have chosen TiN as the underlayer on which the growth catalyst seeds are deposited. Successful growth of carbon nanofibers and nanotubes on the TiN underlayer has already been reported.[6,91–93] More importantly, TiN is known as a conductive diffusion barrier and has been widely used in microelectronic industry for this purpose.[94] Therefore, it allows for using different metals beneath it without being worried of poisoning the catalyst seeds. This is especially important in fabrication of a varactor where the electrical properties of the electrodes are crucial for the device performance. For example, excellent rf

(a)

(b)

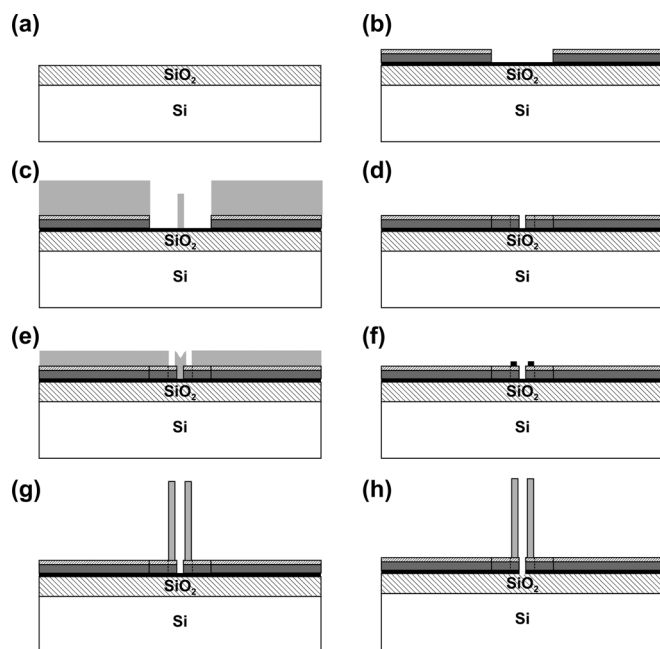**(c)**

(d)

(e)

(f)

(g)

(h)

FIG. 6. Schematic illustration of the process flow for the comblike varactor. (a) The silicon substrate with 400 nm thermally grown silicon dioxide. (b) 5 nm of Cr is deposited first, and then Ti/TiN contact pads are defined on top of it in a photo-lithography step. (c) Dual-layer e-beam resist is spun and patterned. (d) The electrode pattern is transferred to the wafer in a lift-off process. (e) The second dual-layer e-beam resist is spun and patterned. (f) The catalyst seeds pattern is transferred on top of the electrodes in a second lift-off process. (g) The VACNFs are synthesized. (h) The exposed area of the Cr layer is etched in a Cl_2/O_2 reactive ion etching process.
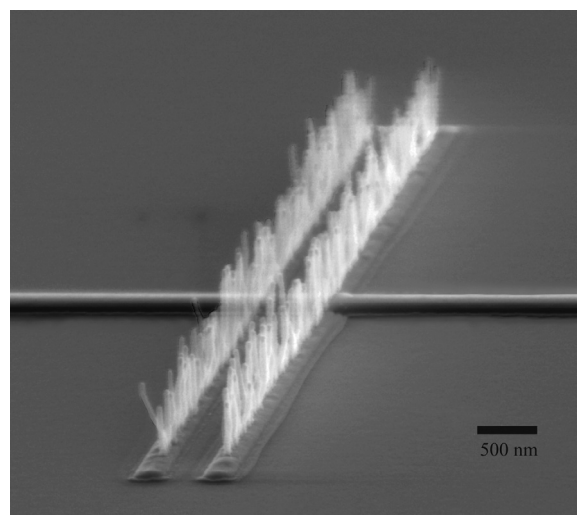

FIG. 7. A SEM micrograph of a comblike varactor taken at sample tilt of 30°. Although the size of the catalyst seeds were precisely controlled using e-beam lithography, the nanofibers uniformity is still very poor both in terms of diameter and height. The electrodes are 10 μm long. The VACNFs are about 80 nm wide and a micrometer long.

materials such as copper and gold, which are not known to yield successful growth, could be incorporated in the device fabrication while buried beneath the diffusion barrier layer. To enhance the adhesion of the TiN layer to the silicon dioxide substrate, Ti was used beneath the TiN layer. We have used a dc PECVD equipment developed in-house to grow the VACNFs. Technical details of the growth equipment can be found elsewhere.[89,95,96]

There exists a large variety of conditions at which VACNFs can be grown by the dc PECVD method. The choice of the growth recipe depends, to a large extent, on the properties of the growth apparatus, the catalyst material, and the metal underlayer. Even in a single growth apparatus for the same catalyst/underlayer combination, there may exist different sets of conditions which all lead to successful growth. The recipe that we found to be most suitable for the synthesis can be divided into three main steps: controlled warm-up, plasma treatment, and growth. In the controlled warm-up, the temperature of the sample was increased from room temperature to 500 °C by 100 °C per minute in NH_3 ambience. The conditions of the warm-up step determine how the catalyst seeds are converted to catalyst nanoparticles.[97,98] After the warm-up step and while the NH_3 ambiance was maintained, the plasma was ignited and the plasma current was set to 20 mA. The ammonia-plasma treatment continued for two minutes during which the temperature of the sample was set to increase from 500 °C to 700 °C (the same temperature slope as before). The purpose of this step was to chemically reduce the native oxide on the catalyst seeds and therefore

enhance the subsequent carbon diffusion during the growth step.[99] Finally, the growth of VACNFs was initiated by introducing acetylene (C_2H_2) as the carbon containing precursor and the growth step continued for twenty minutes.

The fabricated comblike varactor is shown in Fig. 7. Although the nanofibers are grown from predefined Ni seeds all with the same size and thickness, they show a large variation in length and diameter. This poor uniformity leads to an uneven actuation; while the shorter and the thicker nanofibers require a large actuation voltage to bend the thinner and the longer ones snap into contact already at low voltages. The poor growth uniformity has been addressed previously[100] but remains as the major challenge in realizing VACNF-based devices. The fabricated comblike varactor is still far from a functional device.

B. Brushlike varactor

Two types of brushlike varactors with different geometries have been reported in the literature.[38,40] Olofsson *et al.* presented a brushlike varactor with two opposing U-shaped VANTA walls (see Fig. 8).[40] The VANTAs in their varactor were grown on 200 nm thick Mo electrodes with a 10 nm thick Ti adhesion layer. The catalyst layer was composed of 5 nm Al_2O_3 and 1 nm Fe deposited on top of the Mo layer. They grew the nanotubes in a TCVD process at 700 °C and atmospheric pressure using a gas mixture of 5 sccm acetylene, 500 sccm hydrogen, and 500 sccm argon. The resulting nanotubes were multi-walled (typically five walls) with diameters in the range of 5–10 nm and with a length of 135 ± 5 μm. They determined the density of the nanotube arrays from weight measurements, before and after the growth together with geometric information from SEM observations. The VANTAs were found to have a very low density of 10^{10} nanotubes cm^{-2}. Consequently, the U-shape design was chosen to give mechanical stability to thin VANTA walls which otherwise would bend under their own
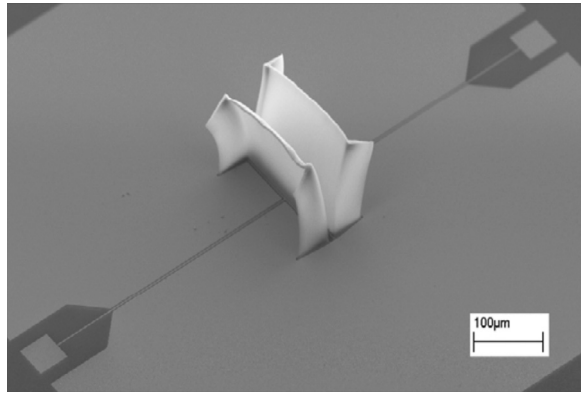
FIG. 8. A SEM micrograph of a brushlike varactor. The VANTA walls have a width of 4 μm, a height of 135 μm, and are separated by 10 μm. Adopted with permission from N. Olofsson, J. Ek-Weis, A. Eriksson, T. Idda, and E. E. B. Campbell, Nanotechnology **20**, 385710 (2009). © 2009, Institute of Physics.

weight. In this way, they expected to achieve an enhanced vertical alignment. However, the VANTA walls still show a non-negligible deformation before actuation takes place.

Arun *et al.* presented an interdigital brushlike varactor with rectangular VANTA structures as shown in Fig. 9.[38] The rectangular shape of the VANTAs was required to provide mechanical stability. In their device, the electrodes were made of 100 nm thick reactively sputtered TiN. The catalyst layer consisted of 1 nm Fe deposited on top of 6 nm Al_2O_3. Their growth process started with a plasma-assisted catalyst pretreatment performed at room temperature and was followed by TCVD synthesis at 580 °C with acetylene as carbon source in H_2/He ambience at 0.4 mbar. The resulting VANTAs were composed of multi-walled nanotubes (typically three walls) with an average diameter of 4 nm and with a length of 50 μm. They determined the density of their VANTA structures to be roughly 10^{12} nanotubes cm^{-2}. Although denser than what was reported by Olofsson *et al.*, the VANTAs still had to be designed in a rectangular shape to provide the required mechanical stability.

V. ASSESSMENT

A. Static capacitance and capacitance density

The equations for static capacitance of the brushlike and the comblike varactors are given in Eq. (1) and Eq. (11),
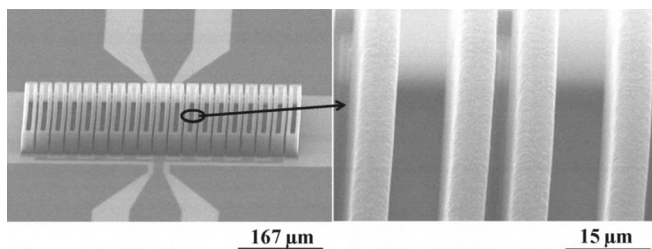

FIG. 9. SEM images of the brushlike varactor by Arun *et al.* The VANTA walls are 7.5 μm thick and are designed in a rectangular shape to enhance their vertical alignment. Adopted with permission from A. Arun *et al.*, *Solid State Device Research Conference ESSDERC '09*, **335** (2009). © 2009, IEEE.

respectively. It is clear that one can always build a larger structure to obtain a larger capacitance. However, in a race for more functionality per unit area, devices with larger capacitance density are preferred. Incompatibility in fabrication requires that MEMS/NEMS varactors are realized on separate dies which gives a drastic increase in total area consumed in a system. Recently, it has been shown that radio frequency MEMS components including varactors can be fabricated in a CMOS compatible process.[101–104] This is more challenging in the case of VANTA- or VACNF-based varactors since the growth on top of a CMOS circuit as a back-end process exposes the electronics to the harsh growth environment with process temperatures exceeding 600 °C. A local heating method has been proposed as a possible solution to grow VANTAs at low ambient temperature with an average temperature of less than 100 °C.[105,106] This method is capable of producing high quality carbon nanotubes, but the lack of control of the growth rate has limited its application so far. The CMOS compatibility of dc PECVD process to synthesize VACNFs has also been assessed[7] and it has been found that if the growth temperature is lowered to 500 °C the level of deterioration in the basic functionality of the electronics becomes negligible. Yet, in both cases, the quality of the resulting materials needs to be improved before they can be incorporated in devices. Thus, the capacitance density of the carbon based varactor remains greatly inferior to its rival technologies as long as the integration issues remain unsolved.

At the time of writing this paper the reported capacitance values of carbon based varactors are still very small.
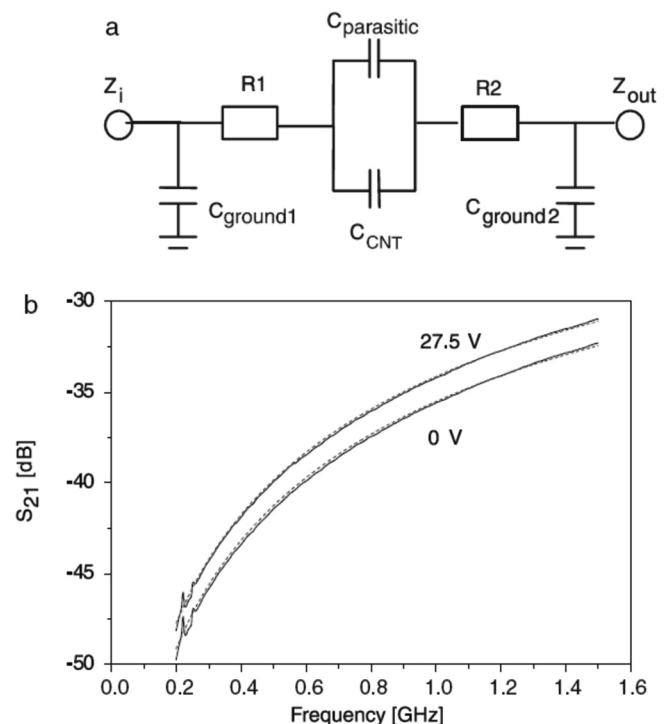

FIG. 10. (a) Equivalent circuit used to fit the experimental results. (b) S21 parameter measured for the frequency range 200 MHz – 1.5 GHz for 0 V and 27.5 V actuation voltages (black line). The equivalent circuit model fits are also shown (red dashed lines). Adopted with permission from N. Olofsson, J. Ek-Weis, A. Eriksson, T. Idda, and E. E. B. Campbell, Nanotechnology **20**, 385710 (2009). © 2009, Institute of Physics.

Olofsson *et al.*, determined the capacitance of their brushlike varactor by measuring the *S*-parameters in the frequency range from 200 MHz to 1.5 GHz. They extracted the values from experimental measurements by considering the equivalent electrical circuit model shown in Fig. 10(a). The results of their measurement are shown in Fig. 10(b) for an actuation voltage of 0 V and 27.5 V. The static capacitance between the nanotube walls was found to be 22.0 fF. The parallel plate capacitance equation, Eq. (1), gives a value of 23.9 fF which is very close to the measured value. The brushlike varactor of Arun *et al.*, presented a higher capacitance value of 200 fF as measured at 4 GHz thanks to its interdigital design.

B. Tunability and parasitic capacitances

The theoretical maximum tunability for an electromechanical parallel plate variable capacitor, as shown in Fig. 4 and discussed earlier, is 50%. The main obstacle to achieve this theoretical maximum is the parasitic capacitances which are added in parallel to the tunable capacitor leading to a reduced tunability. The reduced tunability, C_r, can be expressed by:

$$C_r = \frac{C_{\max}}{C_{\min}} = \frac{C_{tune-\max} + C_f}{C_{tune-\min} + C_f} \quad (17)$$

where $C_{\max}$ and $C_{\min}$ are the total maximum and minimum capacitances, $C_{tune-\max}$ and $C_{tune-\min}$ correspond only to the maximum and minimum values of the tunable capacitor, and C_f denotes the collective contribution of the parasitic capacitances. By applying the parallel plate assumption, Eq. (17) is reduced to:

$$C_r = \frac{C_{tune-\max} + C_f}{C_{tune-\min} + C_f} = \frac{1.5 C_{tune-\min} + \gamma C_{tune-\min}}{C_{tune-\min} + \gamma C_{tune-\min}} = \frac{1.5 + \gamma}{1 + \gamma} \quad (18)$$

Most parallel plate MEMS varactors have $0.15 < \gamma < 0.6$, which yields a capacitance ratio of 27% to 42%.[37] In a carbon based varactor, one can distinguish between two different groups of parasitic capacitances. One group includes capacitances which do not scale with the size of the tunable capacitor such as those originating from contact pads and lines connecting the pads to the main device. A functional varactor must have a minimum tunable capacitance well above the collective value of these parasitic capacitances. In a brush like varactor, the VANTA structures can be grown as tall as 100 μm and more resulting in a relatively large tunable capacitance. However, a comblike varactor consists of VACNFs, which are only a few micrometers tall and therefore the minimum required tunable capacitance must be achieved by designing long rows of nanofibers. In contrast to the first group, the value of the parasitic capacitance between the electrodes on top of which VACNFs or VANTAs are grown increases as the lateral device size increases. This reduces the maximum tunability that can be achieved by carbon based varactors regardless of the size of the tunable capacitor. Again, this reduction is less significant in brushlike varactors due to the relatively large size of the VANTAs

compared to that of the electrodes. Consequently, one would expect maximum tunabilities similar to those of parallel plate MEMS varactors. In order to estimate the maximum tunability in a comblike varactor, one should know the constraints imposed by the fabrication technology as well as the properties of the insulating substrate on top of which the device is fabricated. In the following discussion, we assume device geometries that can be fabricated reproducibly though they may not be the most optimized ones. Moreover, we assume that the device is fabricated on top of silicon dioxide with a relative permittivity of 4.2 (Ref. 107). We have used the finite element method (COMSOL Multiphysics) to compute the parasitic capacitance arising from two parallel metallic electrodes, 300 nm wide and 150 nm thick, deposited on top of silicon dioxide [see Fig. 11(a)]. Then, 3 μm tall and 100 nm wide VACNFs were added on top of the electrodes with 100 nm margin from the edge of the electrodes and the capacitance contribution from the nanofibers was extracted [see Fig. 11(b)]. The reduced tunability was calculated using Eq. (17) from the two computed capacitances as a function of the gap between the electrodes. The result is plotted in Fig. 12. It can be seen that the maximum tunability is reduced from the theoretical 50% to less than 30%. The presence of a maximum at the electrode gap of 150 nm is due to the fact that the VACNFs have been placed at a margin from the edge of the electrodes (the gap between the fibers is 200 nm more than that of the electrodes). We have also taken into account the influence of a conductive substrate beneath the oxide on the tunability. This is a common condition as the oxide layer is usually deposited or grown on top of a conductive substrate such as doped silicon. We calculated the maximum tunability as a function of the oxide thickness both for a grounded and for a floating potential substrate. The result is plotted in Fig. 13. The tunability diminishes to zero as the oxide thickness is reduced. We also observe that the grounded substrate deteriorates the tunability more severely. However, for oxide layers
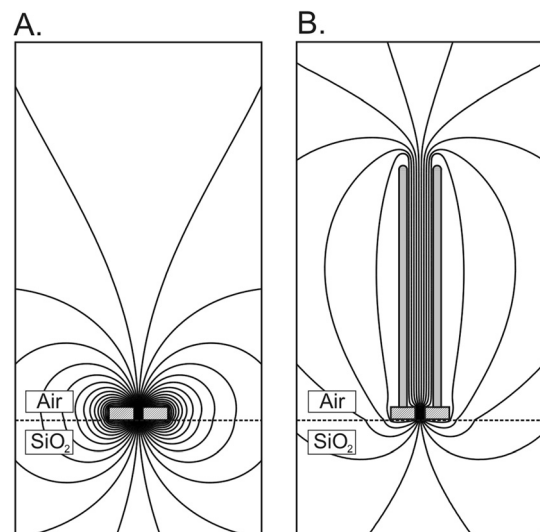

FIG. 11. COMSOL Multiphysics was used to simulate the parasitic capacitance from the electrodes (150 nm thick and 300 nm wide) and the tunable capacitance from the VACNFs (3 μm tall and 100 nm wide). The figure shows the equipotential lines created by (a) only the electrodes and (b) the combination of the electrodes and the VACNFs.
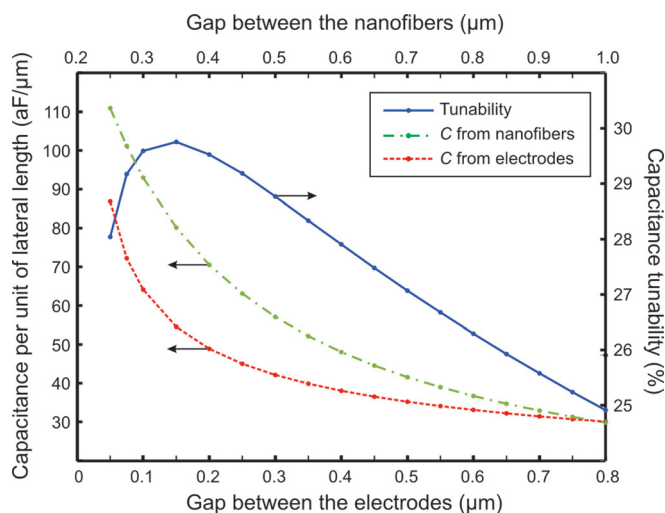
FIG. 12. (Color online) The parasitic capacitance from the electrodes and the tunable capacitance from the VACNFs were computed as a function of the gap between the electrodes. The tuning ratio of a comblike varactor was then calculated using Eq. (17).

thicker than a few micrometers the effect of the substrate becomes negligible.

Olofsson *et al.*, reported a capacitance increase from 22 fF to 27 fF in their brushlike varactor by applying a bias voltage of 27.5 V, shortly before the pull-in voltage was reached.[40] These values correspond only to the tunable capacitor and were measured by de-embedding the parasitic capacitance ($C_{parasitic} = 5.8$ fF). Taking into account the parasitic capacitance, the tunability is calculated using Eq. (17) to be 18%. They also reported that the capacitance could be reproducibly varied up to the value of the pull-in voltage, but when the actuation voltage was increased beyond the pull-in voltage, the VANTA walls collapsed resulting in a sharp decrease in the value of the capacitance after which reproducible behavior could again be observed only with a downward shift in the absolute capacitance of the device.
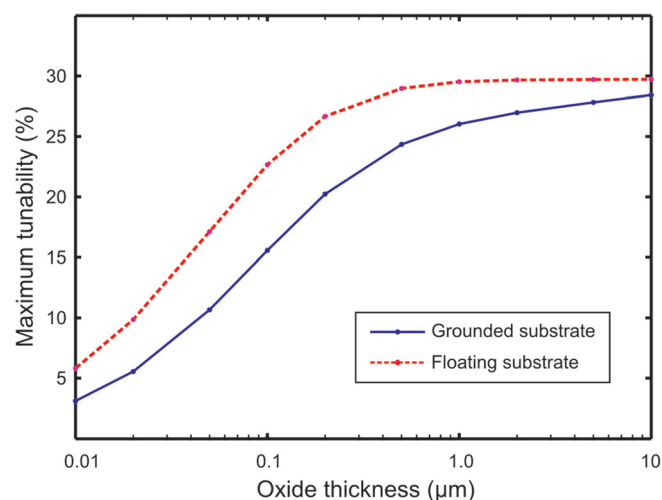

FIG. 13. (Color online) The maximum tunability of a comblike varactor is affected by the presence of a conductive substrate beneath the oxide on top of which the varactor is fabricated. The plot shows the deterioration in the tunability for a grounded and a floating potential substrate as a function of the oxide thickness.

Arun *et al.*, reported a very small tunability of 4% which corresponds to a capacitance increase from 200 fF to 207 fF.[38]

Although no experimental data has been reported yet regarding the tunability of comblike varactors, one should expect lower values based on the previous discussion. This is mainly due to the fact that VANTAs are much larger than VACNFs compared to the electrodes they are grown on. In general, the tunability of carbon based varactors, similar to MEMS parallel plate varactors, is inherently limited compared to capacitance ratio of 4–6 of standard solid-state varactors.[37] However, voltage-controlled oscillators[108,109] and tunable filters[110] have already been demonstrated using the limited tunability of MEMS varactors which show a promise for possible application of the carbon based varactor.

Another important characteristic of the carbon based varactor is its symmetric C-V response. This is due to the fact that the electrostatic force between the opposite electrodes is attractive regardless of the polarity of the applied voltage (see Eq. 4). Consequently, carbon based varactors are never forward biased and hence do not pass current under high-power operation. Moreover, the symmetric C-V response of the carbon based varactor could be exploited to realize frequency multipliers with odd harmonics output as it has been demonstrated using heterostructure barrier varactors with similar C-V response.[34]

C. Quality factor

The quality factor, which indicates the loss in the device, is an important parameter for varactors used in oscillators. In order to investigate the quality factor of a device, one needs to determine the sources of the loss. In a carbon based varactor the losses come from three main sources: the loss in the electrode lines on which the nanostructures are grown, the loss at the interface between the CNTs or the CNFs and the electrode lines, and finally the loss in the CNTs and the CNFs themselves. As was mentioned previously, excellent rf materials such as gold and copper are not known as effective growth underlayers. In order to incorporate these materials in carbon based devices one could deposit a buffer layer between the electrode layer and the catalyst seeds and therefore keep the electrode loss at a minimum. The second source of loss can be assessed using the studies on carbon-metal interfaces. Unlike the near-ohmic characteristic of metal-metal junctions, the contact resistance at the carbon-metal interface dominates the electrical performance of CNT and CNF wires.[111] The possible application of VANTAs and VACNFs as microelectronic interconnects has driven many studies to characterize their end-contact quality.[71,111–115] The reported end-contact resistances vary significantly from one measurement to another suggesting a wide spectrum of influencing parameters. Important parameters are the surface roughness of the metal underlayer as well as its surface oxidation,[115] the wettability of the metal underlayer and its work function,[112] and the growth conditions.[111] In general, the magnitude of the reported contact resistances for an individual interface is in the order of a few to tens of kilo ohms.[111,115] Finally, the intrinsic resistance of individual VACNFs has been measured using the four-point probe measurement method to exclude the effect of contact
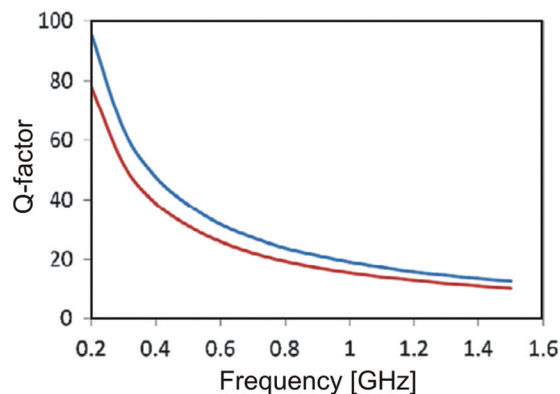
FIG. 14. (Color online) Q-factor extracted from the measured resistance and capacitance as a function of frequency. Upper (blue) line: nonactuated device (0 V), Lower (red) line: actuated device with an applied voltage of 27.5 V between the nanotube walls. Adopted with permission from N. Olofsson, J. Ek-Weis, A. Eriksson, T. Idda, and E. E. B. Campbell, Nanotechnology **20**, 385710 (2009). © 2009, Institute of Physics.

resistance.[116] The VACNFs exhibited linear I-V characteristics with an approximate resistivity of 4.2×10^{-3} $\Omega \cdot$cm which is much smaller than their reported contact resistance. The intrinsic resistance of individual CNTs is many orders of magnitude larger than that of VACNFs since only one (single-walled CNT) or a few (multi-walled CNT) conduction channels or shells are available for electron transport.[117] However, in arrays of VACNFs or in VANTAs a large number of conducting individuals are placed in parallel which dramatically reduces the overall resistance consisting of the intrinsic and the contact resistances. For example Olofsson *et al.*, have measured a series resistance as low as 190 Ω in their brushlike varactor.[40] They extracted the Q-factor of their varactor from measurements. Their results are plotted in Fig. 14 for both nonactuated (0 V) and actuated (27.5 V) cases in the frequency range of 0.2–1.5 GHz. The Q-factor of their device decreases from 100 to 10 as the frequency increases. They believe that the loss in their varactor is dominated by the relatively poor conductance of the sputtered Mo electrodes. The quality factor reported by Arun *et al.*, was as low as 1.7 as measured at 4 GHz. They did not give explanations for the low measured quality factors.[38]

Electromechanical varactors, in general, have the potential of delivering very high Q-factors as no resistive power dissipation occurs in between the oppositely charged electrodes. In solid-state varactors, for example, the tunability is achieved by changing the width of the depletion layer. Realization of the depletion layer with acceptable width depends on a low doped region which creates a high resistance in the signal path leading to a reduced Q-factor. Yet, the demonstration of very high Q-factor carbon based devices has to wait for successful synthesis of VANTAs and VACNFs on top of rf materials with very low contact resistances. Moreover, efforts must be paid to achieve less defective CNTs and CNFs in order to reduce their intrinsic resistances.

D. Operating voltage

The pull-in voltage of the comblike and the brushlike varactors are given by Eq. (14) and Eq. (16), respectively. The pull-in voltage can be used as a good measure for the operating voltage because most of the capacitance change, as seen in Fig. 4, occurs close to this voltage. According to Eq. (14), the pull-in voltage of a comblike varactor depends strongly on the gap between oppositely charged VACNF rows. But this gap is determined by the capacitance requirement and cannot be used freely to tune the operating voltage. This is similar for the height of VACNFs, which is limited by the growth process. The only parameter that can be tuned without considerable effect on other device properties is the diameter of the VACNFs. Therefore, both the device geometry and the growth process conditions are important in determining the operating voltage of a comblike varactor. Based on the device geometries and growth conditions discussed earlier in this paper and taking into account a previous estimation of VACNFs Young's modulus (400 GPa),[118] it should be possible to fabricate comblike varactors with operating voltages in the range of 10 to 30 V. In the case of brushlike varactors, the thickness of the VANTAs can effectively be used to tune the operating voltage. However, the lower limit of the thickness is dictated by the mechanical stability requirements. Jeong *et al.*, have studied the effect of growth geometry on the vertical alignment of VANTAs and showed that for a certain geometry a minimum thickness is required to achieve the necessary mechanical stability and therefore the vertical alignment.[119] Olofsson *et al.*, reported a Young's modulus as low as 3.8 MPa for the VANTAs incorporated in their varactor. This extremely low Young's modulus (lower than that of a rubber) explains why the VANTAs were already bent before applying any bias voltage.[40] Consequently, they added buttresses at the expense of a higher actuation voltage. It is also possible to improve the vertical alignment by growing VANTAs with higher nanotube density but again this will lead to a greater stiffness and hence a larger operating voltage. Similarly, in order to overcome the mechanical stability problem, Arun *et al.*, grew their VANTAs in hollow rectangular structures (see Fig. 9).[39] This limitation increased the operating voltage of the brushlike varactor to $30 - 40$ V in both cases.

Inserting the geometrical data and the estimated Young's modulus from the brushlike varactor fabricated by Olofsson *et al.* into Eq. (16) gives a pull-in voltage as low as 3 V compared to the measured 27.5 V. There are a few reasons behind this underestimation. Generally, the parallel-plate assumption underestimates the pull-in voltage of a base-clamped cantilever system. But the deviation from the parallel plate assumption is much larger here because of the presence of buttresses, which hinder the movements of the plate at the sides. Moreover, the VANTA plates are under an initial stress (slightly bent before the actuation) toward the opposite direction of the actuation, which is not taken into account in the model. It is clear that although the analytical model provides a reliable and cost-effective tool for predicting the behavior of the system, numerical simulations are necessary for accurate modeling of more complicated geometries.

VI. CONCLUSIONS

Recent development in the synthesis of VANTAs and VACNFs has offered an unprecedented opportunity to build

a new class of nano-scale systems; standing nanoelectromechanical devices. Carbon based varactors are among the first emerging systems of this type. Although still in its infancy, the carbon based varactor clearly shows the potential of VANTAs and VACNFs for future applications. In this work, we have presented a simple generic model to describe the behavior of such systems applicable for both comblike and brushlike varactors. The fabrication processes of both devices were also reviewed. Based on the limited published work, it seems that the comblike varactor requires a more demanding fabrication process as the quality of individual VACNFs play an important role in the final device performance. This requires the use of e-beam lithography process and demands a synthesis process capable of producing very uniform VACNFs at a large scale; a functional comblike varactor remains to be demonstrated. On the other hand, functional brushlikes varactors have already been reported. However, the high porosity of VANTAs has resulted in an unexpectedly low mechanical stiffness which has forced the addition of supporting structures such as buttresses.

The performance of the carbon based varactor is still far inferior to its rivals and its journey to maturity is an uneasy ride with a few main obstacles. The first and the foremost is the integration with mainstream CMOS technology. A few attempts have been carried out to achieve this goal, but such an immense objective requires the focus of a large research community. Competitive capacitance densities for carbon based varactors are unreachable unless a successful integration scheme is presented. Another obstacle is the synthesis of VANTAs and VACNFs with low contact resistance on top of rf materials such as copper, most likely by the incorporation of a conductive buffer film such as TiN. Synthesis processes to yield dense VANTAs with large mechanical stiffness and highly uniform VACNFs must also be devised. Yet, the promise of a very high Q-factor, the potential of high power handling due to the capacity of carrying very large currents, the symmetric C-V curve, and the possibility of inexpensive production renders the carbon based NEMS varactor a target worthy of the remaining experimental effort.

ACKNOWLEDGMENTS

[1] C. D. Scott, S. Arepalli, P. Nikolaev, and R. E. Smalley, Appl. Phys. A **72**, 573 (2001).

[2] M. Yudasaka, R. Yamada, N. Sensui, T. Wilkins, T. Ichihashi, and S. Iijima, J. Phys. Chem. B **103**, 6224 (1999).

[3] J. L. Hutchison, N. A. Kiselev, E. P. Krinichnaya, A. V. Krestinin, R. O. Loutfy, A. P. Morawsky, V. E. Muradyan, E. D. Obraztsova, J. Sloan, S. V. Terekhov, and D. N. Zakharov, Carbon **39**, 761 (2001).

[4] Z. J. Shi, Y. F. Lian, X. H. Zhou, Z. N. Gu, Y. G. Zhang, S. Iijima, L. X. Zhou, K. T. Yue, and S. L. Zhang, Carbon **37**, 1449 (1999).

[5] M. Sveningsson, R. E. Morjan, O. A. Nerushev, Y. Sato, J. Backstrom, E. E. B. Campbell, and F. Rohmund, Appl. Phys. A **73**, 409 (2001).

[6] A. M. Rao, D. Jacques, R. C. Haddon, W. Zhu, C. Bower, and S. Jin, Appl. Phys. Lett. **76**, 3813 (2000).

[7] F. A. Ghavanini, H. Le Poche, J. Berg, A. M. Saleem, M. S. Kabir, P. Lundgren, and P. Enoksson, Nano Lett. **8**, 2437 (2008).

[8] K. B. K. Teo, D. B. Hash, R. G. Lacerda, N. L. Rupesinghe, M. S. Bell, S. H. Dalal, D. Bose, T. R. Govindan, B. A. Cruden, M. Chhowalla, G. A. J. Amaratunga, J. M. Meyyappan, and W. I. Milne, Nano Lett. **4**, 921 (2004).

[9] V. Merkulov, A. V. Melechko, M. A. Guillorn, D. H. Lowndes, and M. L. Simpson, Chem. Phys. Lett. **361**, 492 (2002).

[10] V. I. Merkulov, A. V. Melechko, M. A. Guillorn, T. E. McKnight, D. W. Austin, M. Hale, L. Zhang, X. Yang, D. K. Hensley, T. Subich, M. J. Doktycz, D. H. Lowndes, and M. L. Simpson,. Nanotechnology **3**, 66 (2003).

[11] A. V. Melechko, V. I. Merkulov, T. E. McKnight, M. A. Guillorn, K. L. Klein, D. H. Lowndes, and M. L. Simpson, J. Appl. Phys. **97**, 041301 (2005).

[12] S. J. Tans, R. M. Verschueren, and C. Dekker, Nature **393**, 49 (1998).

[13] M. H. Yang, K.B.K. Teo, W. I. Milne, and D. G. Hasko, Appl. Phys. Lett. **87** (2005).

[14] S. G. Wang, J. H. Wang, and J. J. Han, Journal of Wuhan University of Technology-Materials Science Edition **19**, 4 (2004).

[15] L. Wei, R. V. Olivares, L. Qizhen, R. Zhang, M. Kyoung-Sik, and C. P. Wong, *Vertically Aligned Carbon Nanotubes on Copper Substrates for Applications as Thermal Interface Materials: From Synthesis to Assembly* (IEEE, Piscataway, 2009), pp. 441–447.

[16] T. Iwai, H. Shioya, D. Kondo, S. Hirose, A. Kawabata, S. Sato, M. Nihei, T. Kikkawa, K. Joshin, Y. Awano, and N. Yokoyama, *Thermal and Source Bumps Utilizing Carbon Nanotubes for Flip-Chip High Power Amplifiers* (IEEE, Washington DC., 2006), p. 257–260.

[17] M. A. Guillorn, A. V. Melechko, V. I. Merkulov, E. D. Ellis, C. L. Britton, M. L. Simpson, D. H. Lowndes, and L. R. Baylor, Appl. Phys. Lett. **79**, 3506 (2001).

[18] L. R. Baylor, V. I. Merkulov, E. D. Ellis, M. A. Guillorn, D. H. Lowndes, A. V. Melechko, M. L. Simpson, and J. H. Whealton, J. Appl. Phys. **91**, 4602 (2002).

[19] M. A. Guillorn, X. Yang, A. V. Melechko, D. K. Hensley, M. D. Hale, V. I. Merkulov, M. L. Simpson, L. R. Baylor, W. L. Gardner, and D. H. Lowndes, J. Vac. Sci. Technol. B **22**, 35 (2004).

[20] D. G. J. Mann, T. E. McKnight, A. V. Melechko, M. L. Simpson, and G. S. Sayler, Biotechnol. Bioeng. **97**, 680 (2007).

[21] T. E. McKnight, A. V. Melechko, D. K. Hensley, D.G.J. Mann, G. D. Griffin, and M. L. Simpson, Nano Lett. **4**, 1213 (2004).

[22] J. W. Ward, M. Meinhold, B. M. Segal, J. Berg, R. Sen, R. Sivarajan, D. K. Brock, and T. Rueckes, *A Nonvolatile Nanoelectromechanical Memory Element Utilizing a Fabric of Carbon Nanotubes* (IEEE, Orlando, Florida, 2004), pp. 34–38.

[23] C. Hierold, C. Stampfer, T. Helbling, A. Jungen, M. Tripp, and D. Sarangi, in *CNT based Nano Electro Mechanical Systems (NEMS), Nagayo, Japan* (IEEE, Piscataway, 2005), pp. 1–4.

[24] B. Lassagne, Y. Tarakanov, J. Kinaret, D. Garcia-Sanchez, and A. Bachtold, Science **325**, 1107 (2009).

[25] K. Jensen, K. Kim, and A. Zettl, Nat. Nanotechnol. **3**, 533 (2008).

[26] K. Kim, K. Jensen, and A. Zettl, Nano Lett. **9**, 3209 (2009).

[27] A. Eriksson, L. SangWook, A. A. Sourab, A. Isacsson, R. Kaunisto, J. M. Kinaret, and E. E. B. Campbell, Nano Lett. **8**, 1224 (2008).

[28] S. W. Lee, D. S. Lee, R. E. Morjan, S. H. Jhang, M. Sveningsson, O. A. Nerushev, Y. W. Park, and E. E. B. Campbell, Nano Lett. **4**, 2027 (2004).

[29] S. Axelsson, E. E. B. Campbell, L. M. Jonsson, J. Kinaret, S. W. Lee, Y. W. Park, and M. Sveningsson, New J. Phys. **7** (2005).

[30] D. S. Lee, J. Svensson, S. W. Lee, Y. W. Park, and E. E. B. Campbell, J. Nanosci. Nanotechnol. **6**, 1325 (2006).

[31] J. E. Jang, S. N. Cha, Y. Choi, G. A. J. Amaratunga, D. J. Kang, D. G. Hasko, J. E. Jung, and J. M. Kim, Appl. Phys. Lett. **87**, 163114 (2005).

[32] J. E. Jang, S. N. Cha, Y. J. Choi, D. J. Kang, T. P. Butler, D. G. Hasko, J. E. Jung, J. M. Kim, and G. A. J. Amaratunga, Nat. Nanotechnol. **3**, 26 (2008).

[33] P. Andreani and S. Mattisson, Analog Integr. Circuits and Signal Process. **22**, 17 (2000).

[34] L. Dillner, J. Stake, and E. L. Kollberg, Microwave Opt. Technol. Lett. **15**, 26 (1997).

[35] A. Dec and K. Suyama, IRE Trans. Microwave Theory Tech. **46**, 2587 (1998).

[36] N. Hoivik, M. A. Michalicek, Y. C. Lee, K. C. Gupta, and V. M. Bright, in *2001 IEEE Mtt-S International Microwave Symposium Digest*, edited by B. Sigmon, (IEEE, Phoenix, AZ, 2001), pp. 2115–2118.

[37]G. M. Rebeiz, *R. F. MEMS Theory, Design, and Technology* (Wiley, New York, 2003).

[38]A. Arun, D. Acquaviva, M. Fernandez-Bolanosa, P. Salet, H. Le-Poche, T. Idda, R. Smajda, A. Magrezb, L. Forro, and A. M. Ionescu, in *Micro-Electro-Mechanical Capacitors Based on Vertical Carbon Nanotube Arrays* (IEEE, Piscataway, 2003), pp. 335–338.

[39]D. Dragoman and M. Dragoman, J. Appl. Phys. **101** (2007).

[40]N. Olofsson, J. Ek-Weis, A. Eriksson, T. Idda, and E. E. B. Campbell, Nanotechnology **20**, 385710 (2009).

[41]J. Ek-Weis, A. Eriksson, T. Idda, N. Olofsson, and E. E. B. Campbell, J. Nanoeng. Nanosyst. **222**, 111 (2008).

[42]T. Ricart, S. Pacchini, C. S. Cojocaru, D. Pribat, D. Dubuc, and K. Grenier, in *Carbon Nanotubes and Associated Devices*, edited by M. Razeghi, D. Pribat, and Y. H. Lee, (SPIE, Bellingham, WA, 2008), p. F370.

[43]S. Pacchini, M. Dilhan, T. Ricart, C. Cojocaru, D. Pribat, D. Dubuc, and K. Grenier, in *Carbon Nanotubes and Associated Devices*, edited by M. Razeghi, D. Pribat, and Y. H. Lee (2008), p. 3719.

[44]D. K. Cheng, *Fundamentals of Engineering Electromagnetics* (Addison-Wesley, Reading, MA, 1993).

[45]M. P. J. Tiggelman, K. Reimann, F. Van Rijs, J. Schmitz, and R. J. E. Hueting, IEEE Trans. Electron Devices **56**, 2128 (2009).

[46]B. Gelmont, M. Shur, and R. J. Mattauch, IRE Trans. Microwave Theory Tech. **39**, 857 (1991).

[47]W. Shockley, Bell Syst. Tech. J. **28**, 435 (1949).

[48]E. Kollberg and A. Rydberg, Electron. Lett. **25**, 1696–1698 (1989).

[49]A. K. Tagantsev, V. O. Sherman, K. F. Astafiev, J. Venkatesh, and N. Setter, J. Electroceram. **11**, 5 (2003).

[50]A. Dec and K. Suyama, IRE Trans. Microwave Theory Tech. **48**, 1943 (2000).

[51]D. J. Young and B. E. Boser, IEEE, *A Micromachine-Based RF Low-Noise Voltage-Controlled Oscillator* (IEEE, Santa Clara, CA, 1997), pp. 431–434.

[52]J. B. Yoon and C.T.C. Nguyen, *A High-Q Tunable Micromechanical Capacitor with Movable Dielectric for RF Applications* (IEEE, San Francisco, CA, 2000), pp. 489–492.

[53]R. L. Borwick, PP. A. Stupar, J. F. DeNatale, R. Anderson, and R. Erlandson, IRE Trans. Microwave Theory Tech. **51**, 315 (2003).

[54]R. L. Borwick, P. A. Stupar, J. DeNatale, R. Anderson, C. L. Tsai, and K. Garrett, in *Fifteenth IEEE International Conference on Micro Electro Mechanical Systems* (IEEE, Las Vegas, NV, 2002), pp. 669–672.

[55]P. Kim and C. M. Lieber, Science **286**, 2148 (1999).

[56]B. A. Cruden and A. M. Cassell, IEEE Trans. Nanotechnol. **5**, 350 (2006).

[57]S. Akita and Y. Nakayama, Japanese Journal of Applied Physics, Part 1: Regular Papers and Short Notes and Review Papers **41**, 4242 (2002).

[58]S. Akita, Y. Nakayama, S. Mizooka, Y. Takano, T. Okawa, Y. Miyatake, S. Yamanaka, M. Tsuji, and T. Nosaka, Appl. Phys. Lett. **79**, 1691 (2001).

[59]M. Dequesnes, S. V. Rotkin, and N. R. Aluru, Nanotechnology **13**, 120 (2002).

[60]M. Dequesnes, Z. Tang, and N. R. Aluru,. ASME J. Eng. Mater. Technol. **126**, 230 (2004).

[61]J. E. Jang, S. N. Cha, Y. Choi, T. P. Butler, D. J. Kang, D. G. Hasko, J. E. Jung, Y. W. Jin, J. M. Kim, and G.A.J. Amaratunga, Appl. Phys. Lett. **93**, 113105 (2008).

[62]H. Cui, X. Yang, M. L. Simpson, D. H. Lowndes, and M. Varela, Appl. Phys. Lett. **84**, 4077 (2004).

[63]A. V. Melechko, V. I. Merkulov, T. E. McKnight, M. A. Guillorn, K. L. Klein, D. H. Lowndes, and M. L. Simpson, J. Appl. Phys. **97**, 041301 (2005).

[64]J. E. Jang, S. N. Cha, Y. Choi, D. J. Kang, T. P. Butler, D. G. Hasko, J. E. Jung, J. M. Kim, and G. A. J. Amaratunga, in *Nanotube Based Vertical Nano-Devices for High Integration Density* (IEEE, Piscataway, 2006) pp. 89–92.

[65]J. E. Jang, S. N. Cha, Y. Choi, D. J. Kang, T. P. Butler, D. G. Hasko, J. M. Kim, and G. A. J. Amaratunga, in *CNT Based Mechanical Devices for ULSI Memory* (IEEE, Piscataway, 2006), pp. 461–464.

[66]J. Lee and S. Kim,. Sens. Actuators, A **120**, 193 (2005).

[67]J. M. Kinaret, T. Nord, and S. Viefers, Appl. Phys. Lett. **82**, 1287 (2003).

[68]C. H. Ke, N. Pugno, B. Peng, and H. D. Espinosa, J. Mech. Phys.Solids **53**, 1314 (2005).

[69]F. F. Zhang, X. L. Wang, C. X. Li, X. H. Li, Q. Wan, Y. Z. Xian, L. T. Jin, and K. Yamamoto, Anal. Bioanal. Chem. **382**, 1368 (2005).

[70]J. Li, R. Stevens, L. Delzeit, H. T. Ng, A. Cassell, J. Hah, and M. Meyyappan, Appl. Phys. Lett. **81**, 910 (2002).

[71]J. Li, Q. Ye, A. Cassell, H. T. Ng, R. Stevens, J. Han, and M. Meyyappan, Appl. Phys. Lett. **82**, 2491 (2003).

[72]Z. H. Yang, Q. W. Wang, J. L. Wang, Z. F. Li, and S. B. Sang, Mater. Lett. **61**, 3103 (2007).

[73]B. Zhao, D. N. Futaba, S. Yasuda, M. Akoshima, T. Yamada, and K. Hata, ACS Nano **3**, 108 (2009).

[74]S. S. Fan, M. G. Chapline, N. R. Franklin, T. W. Tombler, A. M. Cassell, and H. J. Dai, Science **283**, 512 (1999).

[75]A. Isacsson and J. M. Kinaret, Phys. Rev. B **79**, 165418 (2009).

[76]M. Y. A. Yousif, P. Lundgren, F. Ghavanini, P. Enoksson, and S. Bengtsson, Nanotechnology **19**, 285204 (2008).

[77]A. Y. Cao, P. L. Dickrell, W. G. Sawyer, M. N. Ghasemi-Nejhad, and P. M. Ajayan, Science **310**, 1307 (2005).

[78]M.-H. Bao, *Micro Mechanical Transducers* (Elsevier, 2000), Vol. **8**.

[79]Z. F. Ren, Z. P. Huang, J. W. Xu, J. H. Wang, P. Bush, M. P. Siegal, and P. N. Provencio, Science **282**, 1105 (1998).

[80]B. O. Boskovic, V. Stolojan, R.U.A. Khan, S. Haq, and S.R.P. Silva, Nat. Mater. **1**, 165 (2002).

[81]H. Le Poche, J. Dijon, and T. Goislard de Monsabert, Carbon **45**, 2904 (2007).

[82]L. Delzeit, I. McAninch, B. A. Cruden, D. Hash, B. Chen, J. Han, and M. Meyyappan, J. Appl. Phys. **91**, 6027 (2002).

[83]C. Bower, O. Zhou, W. Zhu, D. J. Werder, and S. H. Jin, Appl. Phys. Lett. **77**, 2767 (2000).

[84]A. V. Melechko, R. Desikan, T. E. McKnight, K. L. Klein, and P. D. Rack, J. Phys. D **42**, 193001 (2009).

[85]M. Meyyappan, L. Delzeit, A. Cassell, and D. Hash,. Plasma Sources Sci. Technol. **12**, 205 (2003).

[86]M. A. Guillorn, T. E. McKnight, A. Melechko, V. I. Merkulov, P. F. Britt, D. W. Austin, D. H. Lowndes, and M. L. Simpson, J. Appl. Phys. **91**, 3824 (2002).

[87]F. A. Ghavanini, Ph. D thesis, Chalmers University of Technology, 2009.

[88]V. I. Merkulov, D. H. Lowndes, Y. Y. Wei, G. Eres, and E. Voelkl, Appl. Phys. Lett. **76**, 3555 (2000).

[89]M. S. Kabir, R. E. Morjan, O. A. Nerushev, P. Lundgren, S. Bengtsson, P. Enoksson, and E. E. B. Campbell, Nanotechnology **17**, 790 (2006).

[90]M. Dubosc, S. Casimirius, M. P. Besland, C. Cardinaud, A. Granier, J. L. Duvail, A. Gohier, T. Minea, V. Arnal, and J. Torres, Microelectron. Eng. **84**, 2501 (2007).

[91]J. H. Han, T. Y. Lee, D. Y. Kim, J. B. Yoo, C. Y. Park, J. J. Choi, T. Jung, I. T. Han, J. E. Jung, and J. M. Kim, J. Vac. Sci. Technol. B **22**, 1636 (2004).

[92]J. H. Han, T. Y. Lee, D. Y. Kim, J. B. Yoo, C. Y. Park, J. J. Choi, T. Jung, I. T. Han, and J. M. Kim, Diamond Relat. Mater. **13**, 987 (2004).

[93]F. Le Normand, C. T. Fleaca, A. Gulas, A. Senger, O. Ersen, I. N. Mihailescu, G. Socol, D. Muller, and M.C.M. de Lucas, J. Mater. Res. **23**, 619 (2008).

[94]C. Jiménez, J. Perrière, C. Palacio, J. P. Enard, and J. M. Albella, Thin Solid Films **228**, 247 (1993).

[95]R. E. Morjan, Ph. D.thesis, Chalmers University of Technology, 2006.

[96]R. E. Morjan, V. Maltsev, O. Nerushev, Y. Yao, L. K. L. Falk, and E. E. B. Campbell, Chem. Phys. Lett. **383**, 385 (2004).

[97]M. Chhowalla, K. B. K. Teo, C. Ducati, N. L. Rupesinghe, G. A. J. Amaratunga, A. C. Ferrari, D. Roy, J. Robertson, and W. I. Milne, J. Appl. Phys. **90**, 5308 (2001).

[98]M. S. Bell, K.B.K. Teo, and W. I. Milne, J. Phys. D **40**, 2285 (2007).

[99]S. J. Randolph, J. D. Fowlkes, A. V. Melechko, K. L. Klein, H. M. Meyer, M. L. Simpson, and P. D. Rack, Nanotechnology **18**, 465304 (2007).

[100]K. B. K. Teo, S. B. Lee, M. Chhowalla, V. Semet, B. Vu Thien, O. Groening, M. Castignolles, A. Loiseau, G. Pirio, P. Legagneux, D. Pribat, D. G. Hasko, H. Ahmed, G. A. J. Amaratunga, and W. I. Milne, in *Plasma Enhanced Chemical Vapour Deposition Carbon Nanotubes/Nanofibres-How uUniformDo They Grow?* (IOP Publishing, UK, 2003), pp. 204–211.

[101]S. Fouladi, M. Bakri-Kassem, and R. R. Mansour, in *An Integrated Tunable Band-Pass Filter Using MEMS Parallel-Plate Variable Capacitors Implemented with 0.35 m CMOS Technology* (IEEE, Piscataway, 2007) pp. 505–508.

[102]B. Lacroix, A. Pothier, A. Crunteanu, C. Cibert, F. Dumas-Bouchiat, C. Champeaux, A. Catherinot, and P. Blondy, in *CMOS Compatible Fast Switching RF MEMS Varactors* (IEEE, Piscataway, 2006), p. 4.

[103] J. E. Ramstad, K. G. Kjelgaard, B. E. Nordboe, and O. Soeraasen, in *RF MEMS Front-End Resonator, Filters, Varactors and a Switch Using a CMOS-MEMS Process* (IEEE, Piscataway, 2009), p. 6.

[104] T. Vaha-Heikkila and M. Ylonen, IRE Trans. Microwave Theory Tech. **56**, 720 (2008).

[105] S. Dittmer, S. Mudgal, O. A. Nerushev, and E.E.B. Campbell, Low Temp. Phys. **34**, 834 (2008).

[106] S. Dittmer, O. A. Nerushev, and E. E. B. Campbell, Appl. Phys. A **84**, 243 (2006).

[107] J. D. Plummer, M. D. Deal, and P. B. Griffin, *Silicon VLSI Technology; Fundamentals, Practice and Modeling* (Prentice Hall, Englewood Cliffs, 2000).

[108] D. J. Young, B. E. Boser, V. Malba, and A. F. Bernhardt, Int. J. RF f Microwave Comput.-Aided Eng. **11**, 285 (2001).

[109] A. Dec and K. Suyama, IRE Trans. Microwave Theory Tech. **48**, 1943 (2000).

[110] A. Abbaspour-Tamijani, L. Dussopt, and G. M. Rebeiz, IRE Trans. Microwave Theory Tech. **51**, 1878 (2003).

[111] Q. Ngo, D. Petranovic, S. Krishnan, A. M. Cassell, Q. Ye, J. Li, M. Meyyappan, and C. Y. Yang, IEEE Trans. Nanotechnol. **3**, 311 (2004).

[112] S. C. Lim, J. H. Jang, D. J. Bae, G. H. Han, S. Lee, I. S. Yeo, and Y. H. Lee, Appl. Phys. Lett. **95**, 264103 (2009).

[113] A. M. Cassell, J. Li, R. M. D. Stevens, J. E. Koehne, L. Delzeit, H. T. Ng, Q. Ye, J. Han, and M. Meyyappan, Appl. Phys. Lett. **85**, 2364 (2004).

[114] X. J. Yang, M. A. Guillorn, D. Austin, A. V. Melechko, H. T. Cui, H. M. Meyer, V. I. Merkulov, J.B.O. Caughman, D. H. Lowndes, and M. L. Simpson, Nano Lett. **3**, 114305 (2003).

[115] L. Fourdrinier, H. Le Poche, N. Chevalier, D. Mariolle, and E. Rouviere, J. Appl. Phys. **104**, 114305 (2008).

[116] L. Zhang, D. Austin, V. I. Merkulov, A. V. Meleshko, K. L. Klein, M. A. Guillorn, D. H. Lowndes, and M. L. Simpson, Appl. Phys. Lett. **84**, 3972 (2004).

[117] S. Frank, P. Poncharal, Z. L. Wang, and W. A. de Heer, Science **280**, 1744 (1998).

[118] A. Eriksson, S. Lee, A. A. Sourab, A. Isacsson, R. Kaunisto, J. M. Kinaret, and E. E. B. Campbell, Nano Lett. **8**, 1224 (2008).

[119] G. H. Jeong, N. Olofsson, L. K. L. Falk, and E. E. B. Campbell, Carbon **47**, 696 (2009).